Durability of Cementitious Grouts in Cold Climates

Arjun Jayaprakash[a,*], James M. Nau[a], Mohammad Pour-Ghaz[a], Mervyn J. Kowalsky[a]

[a]*North Carolina State University, Department of Civil, Construction, and Environmental Engineering, Box 7908, Raleigh, NC 27695, USA*

Abstract

The grouted shear stud (GSS) connection for steel bridge substructures was developed as a ductile alternative to directly welded column-to-cap-beam connections. During an earthquake, the GSS connection relocates the plastic hinge to the bridge column and eliminates brittle cracking at the weld region thereby providing full strength and ductility capacity. However, the grout material used for fabrication of the GSS connection is susceptible to damage through years of exposure, especially to extreme cold climates. This paper presents a study conducted to evaluate the durability of the grout material in cold-climates. A series of experiments was performed to ascertain the durability of commonly available high-strength cementitious grouts. While there were grouts that exhibited good durability, inconsistencies within the material were observed.

Keywords: Steel bridge substructures, Grouted shear stud connection, Socket connection, Grout durability, Physical damage simulation

1. Introduction

1.1. Development of the GSS connection

The use of structural systems consisting of hollow circular steel piles directly welded to HP or W-shape cap beams has been widespread. Fulmer et al. [1, 2] investigated multiple weld configurations that are typically used to connect pipe columns to cap beams. These were fillet weld, complete joint penetration (CJP) weld, CJP weld with a reinforcing fillet outside the pipe, and CJP weld with reinforcing fillets both inside and outside the pipe. Irrespective of the weld configuration, undesirable brittle cracking at the weld or the heat affected zones in the pile was observed. They concluded that while welding steel pipe columns to cap beams may be acceptable for non-seismic applications, using such a connection in seismic design without explicit consideration for the protection of welded regions results in undesirable brittle mode of failure.

The grouted shear stud (GSS) connection for steel bridge substructures was developed by Fulmer et al. [3] as a ductile alternative to directly welded column-to-cap-beam connections. The GSS connection is an external socket-type connection that consists of a prefabricated cap beam to which a pipe stub is welded, as shown in Figure 1a. The stub pipe, larger in diameter than the column,

*Corresponding author

Email addresses: ajayapr@ncsu.edu (Arjun Jayaprakash), nau@ncsu.edu (James M. Nau), mpourgh@ncsu.edu (Mohammad Pour-Ghaz), kowalsky@ncsu.edu (Mervyn J. Kowalsky)

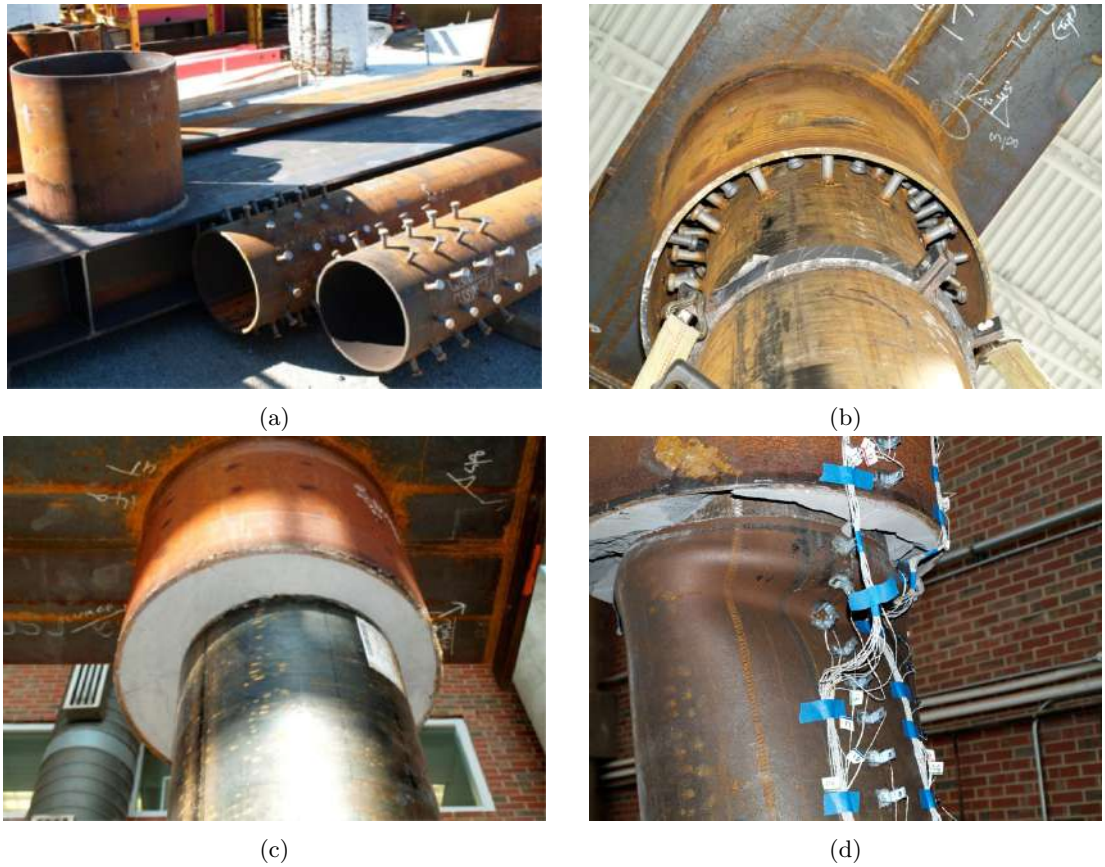

Figure 1: Stages of the GSS connection: (a) Constituent components, (b) Connection before grouting, (c) Connection after grouting, (d) Failure by plastic hinge relocation.

acts as a socket into which the column can be inserted. In Figure 1a, the cap beam is shown on the left, resting on its top surface. The inner wall of the stub pipe shown in the figure contains 12 vertical lines of 3/4" diameter shear studs. Similarly, the top of each pile section had 12 lines of studs, as shown in Figure 1a.

In the field, shear studs are welded to the pile after driving and cutting it at the proper elevation. No additional field welding is required in the construction of the GSS connection. After inserting the pile in the stub (Figure 1b), the moment resisting connection is completed by pumping a flowable non-shrink high-strength grout into the annular region (Figure 1c). Fulmer et al. [3] tested two-column steel bents that use the GSS connection by subjecting them to cyclic quasi-static lateral loading. These tests showed that the GSS connection can successfully protect the welded region by relocating the plastic hinge formation to the steel column (Figure 1d) below the larger diameter pipe stub. Moreover, the GSS connection also provided increased system strength and displacement capacity in comparison to the directly welded connections.

1.2. Advantages of the GSS connection

The GSS connection enables a designer to make efficient use of column moment and ductility capacity. Using capacity design principles, one can ensure that the connection remains protected and the column be the weakest link. Consequently, the GSS connection eliminates premature brittle failure modes such as cracking at the weld or heat affected zone.

The GSS connection can also be employed within accelerated bridge construction (ABC) for steel bridge substructures. The cap beam with pipe stub sockets can be pre-fabricated and brought to the site where it can be lowered onto the driven piles until the bottom of the cap beam bears on the pile top. The connection can then be formed and pumped with commercially available grout in little time to complete the construction process. The time required for field welding and welding inspection under conventional construction processes is mostly eliminated.

Although the GSS connection was developed for new construction, it can be readily adapted for retrofitting of steel bridges in which column to cap beam connections are deficient. To accomplish this retrofit, the pipe stub can be cut longitudinally to produce two semicircular half-stub sections. Shear studs can then be welded on the inside of these half-stubs and to the top of an existing column. The half-stub sections can then be brought together from opposite sides of the column, welded to the existing cap beam, and then welded to each other prior to grouting. While there is field welding to be performed, these welds are capacity protected, ensuring their satisfactory performance.

The structural performance of systems incorporating the GSS connection has high tolerance to construction errors. Fulmer et al. [3] compared the performance of two specimens with GSS connections where the first specimen had concentric columns and stubs, while the second had columns that were offset with respect to the stub. Both systems performed comparably under cyclic quasi-static lateral loading protocols.

Finally, the GSS connection can be employed irrespective of the structural system, i.e., in steel, reinforced concrete, or reinforced concrete filled steel tube bridge piers. The underlying mechanism of the GSS connection is plastic hinge relocation. This mechanism is independent of the structural system.

1.3. Motivation for this study

The GSS connection is demonstrably ideal for deployment in regions of high seismicity. Tests performed on the GSS connection by Fulmer et al. [3] have shown that a high-strength grout can successfully transfer the forces and relocate the plastic hinge to the column. However, these tests were performed in laboratory conditions on specimens with new and undamaged grout. In reality, bridges are exposed to a variety of extreme environments for many years. If engineers are to use the GSS connection in practice, they must expect some amount of grout deterioration. For example, a geographical area of interest for practical application of the GSS connection is the state of Alaska, United States. While Alaska falls in a high-seismic zone, it is also dominated by sub-zero temperatures for major portions of the year. To deploy the GSS connection in such a region, cold climate durability of the connection becomes an important consideration.

The use of grout makes the construction of the GSS connection rapid, which is desirable because of short construction seasons in Alaska. However, during the service life of a bridge, these connections are exposed to a large number of low temperature events, thermal gradients, and freeze-thaw (FT) cycles. These environmental conditions may adversely affect the performance of the connection due to mechanical degradation, i.e., cracking of the grout [4, 5, 6]. Cyclic freezing and thawing can result in damage and degradation of concrete in the presence of a sufficient amount of moisture

in its pore structure [5, 6, 7]. The component of concrete largely vulnerable to freeze and thaw damage is the cement paste, which is a combination of cement and water. Cumulative expansion and collection of water within the grout microstructure during FT cycles induce tensile stresses and cause cracking in the paste when these stresses exceed the tensile strength of the hardened cement paste [5, 8, 9]. In addition, the circular geometry of the connection and the presence of shear studs were thought to also contribute to degradation of the grout because they provide restraint against free shrinkage [10, 11].

Properly designed grouts can withstand a large number of FT cycles without degradation [6, 12]. The goal of this study was to investigate whether the factors listed above pose significant concerns to the durability of the grout material within the GSS connection.

This study evaluated the durability of commercially available cementitious grouts in extreme cold climates. Durability of any material is only meaningful within the context of a specific geographical area and a particular application [4]. In porous materials such as concrete or grout, water is generally involved in every form of deterioration and the ease of penetration of water into the solid usually determines the rate of deterioration. Durability under one set of conditions does not equate to durability under another, and therefore it is important to specify a target environmental condition before proceeding with durability determination.

2. Grout Durability Tests

Durability of concrete has been widely studied, and there exist standard test procedures to evaluate the durability of different concrete mixtures. We assumed that grouts are different from concrete only with respect to the absence of coarse aggregates. Both are porous materials, and therefore the standard test methods to evaluate degradation of one can be applied to the other. In the specific application of the GSS connection, two major issues that can potentially cause degradation and in turn cracking of the grout material in Alaskan cold climates are freeze and thaw cracking [4, 6, 7, 12, 13, 14], and restrained shrinkage cracking [10, 11, 15, 16, 17].

2.1. Freeze-Thaw Cracking of Cementitious Grouts

Concrete is made up of four main components: cement, water, fine aggregates, and coarse aggregates. The mixture of cement and water, also known as cement paste, binds the aggregates together to form structural concrete. Cyclic freezing and thawing can result in damage and degradation of the cement paste in the presence of sufficient amount of moisture in its pore structure.

Variations of freeze-thaw test methods have emerged over time. Albeit different in other aspects, all of the test methods follow the same core principle. Material specimens are subjected to freezing and thawing for a predetermined number of cycles. The most widely used freeze-thaw test method is ASTM C666 [18]. It is an accelerated test method in which specimens are subjected to a maximum of 300 freeze-thaw cycles. ASTM C666 is especially useful for the comparison of freeze-thaw vulnerability of different materials.

Investigating the durability of all commercial cementitious grouts was as expensive as it was fruitless. First, there are a myriad of competing manufacturers that produce similar products. To procure each one of them was expensive. Second, the chemical composition of every grout is proprietary, and the grouts are constantly being modified by the manufacturers. Results obtained now may not reflect their characteristics after a few years. Third, standard durability tests on cementitious materials specific to cold climate exposure take an extremely long time to perform. Testing one batch of specimens according to ASTM C666 may take up to 75 to 80 days to complete.

With due consideration of all of the aforementioned issues, few commercial grouts meeting AKDOT specifications were chosen to be investigated to obtain some information on the suitability of these grouts.

In this study, four commonly available commercial grouts were tested according to ASTM C666 Procedure A. These grouts were named CG1 through CG4 as shown in Table 1. These grouts were chosen because they had been approved by AKDOT&PF as they met their specifications. The grouts were high-strength cementitious grouts. Figure 2 shows the cylinder strength of these grouts measured according to ASTM C39 [19] and the cube strength measured according to ASTM C109 [20]. Note that the cubes for CG3 show almost equal strength at all ages, a result which is not consistent with the cylinders from the same batch. A likely reason for this is improper curing. Cubes of CG3 grout were not sealed after demolding due to misplacement. Drying ensued preventing further hydration. This drying halted strength gain. We want to emphasize the importance of curing for strength test samples, especially for cubic specimens since they can lose a significant amount of moisture rapidly. Data from other grouts, which were cured without moisture loss, show an increase in strength with age.

Table 1: Material used, bag weights, and the amount of water added in each mixture

Material	**Bag Weight (lbs.)**	**Water added per bag (lbs.)**	**Consistency label***
CG1	55	8.5	Plastic-Flowable
CG2	50	8.4	Flowable
CG3	50	6.6	Flowable
CG4	50	9.3	Flowable

* Label specified by manufacturer corresponding to the amount of water

The freeze-thaw specimens were 3"×3"×12" prismatic beams prepared in steel molds as shown in Figure 3. These specimens were cured under saturated lime water for 14 days after demolding. Identical specimens were required as controls to monitor the temperature inside the material during the testing because ASTM C666 specifies the control of the core temperature of the samples rather than the ambient temperature. Thermocouples were embedded within the control specimens for continuous acquisition of temperature data. A cycle period of 6 hours was used which enabled 4 cycles per day. The specimens were submerged in water throughout the test and were kept in steel trays that were fabricated in-house meeting ASTM requirements, as shown in Figure 4a. The specimens were subjected to FT cycles between 40 ± 3 °F (4 ± 2 °C) and 0 ± 3 °F (-18 ± 2 °C) in an environmental chamber (Figure 4b) that was capable of being programmed with a pre-defined temperature cycle. A typical temperature cycle for the control specimens and the chamber air is shown in Figure 5.

ASTM C666 specifies to assess material damage by monitoring the reduction in its relative dynamic elastic modulus (RDME). This was done in the following manner. The fundamental frequency of all specimens was measured at 40°F (4°C) prior to subjecting them to testing. During testing, the specimens were removed from the chamber at intervals of no greater than 36 cycles to measure their fundamental frequency. Since the dynamic elastic modulus of the material is directly proportional to the square of its fundamental frequency (Equation 1), the ratio of the squares of the frequencies is equal to the RDME as shown in Equation 2. The results were plotted in a graph

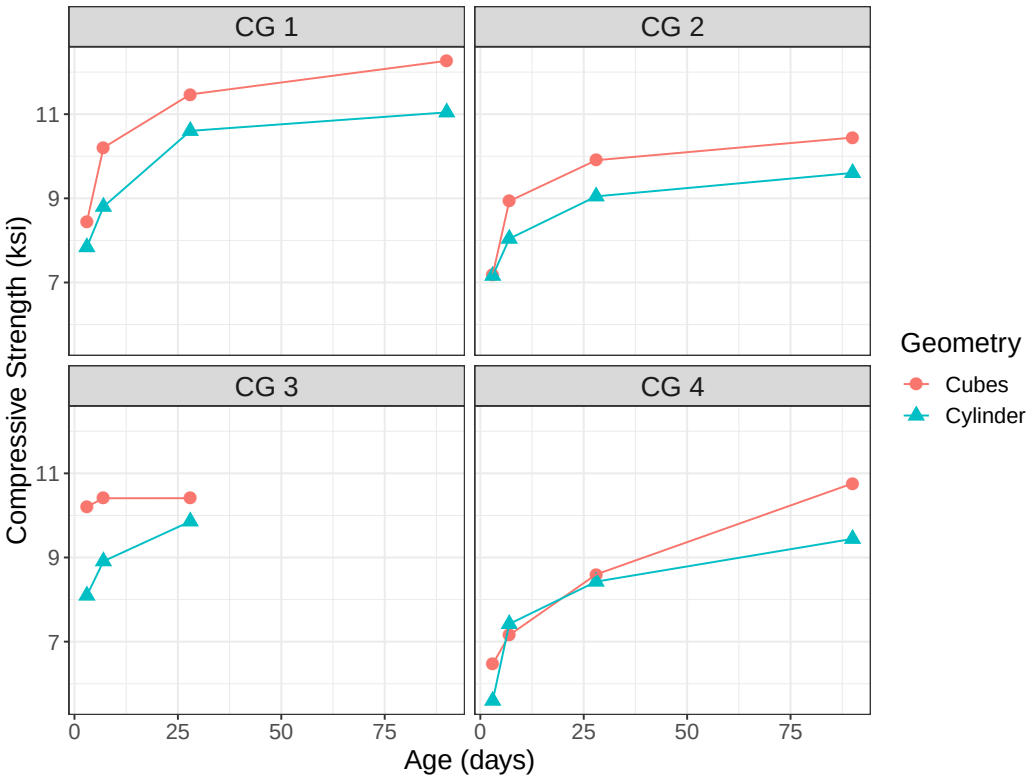

Figure 2: Comparison of cube strength and cylinder strength for all the tested grouts.

with the number of cycles on the x-axis and RDME (E_N/E_0) on the y-axis. Specimen damage is represented by a decrease in RDME as the number of cycles increase. Note that the term RDME and the ratio E_N/E_0 have been used interchangeably in this document.

$$E_D \propto f^2 \tag{1}$$

$$\frac{E_N}{E_0} = \frac{f_N^2}{f_0^2} \tag{2}$$

where,

E_D = Dynamic Elastic Modulus
E_N = Dynamic Elastic Modulus after N cycles
E_0 = Initial Dynamic Elastic Modulus
f_N = Fundamental frequency after N cycles
f_0 = Initial fundamental frequency

Measurement of the fundamental frequency of prismatic specimens was carried out according to ASTM C215 [21]. The setup is shown in Figure 6. An accelerometer was attached to one of the ends of the specimen. The specimen was then placed on a damping mat and was impacted at the center with a hammer. The acceleration response of the specimen was recorded by an

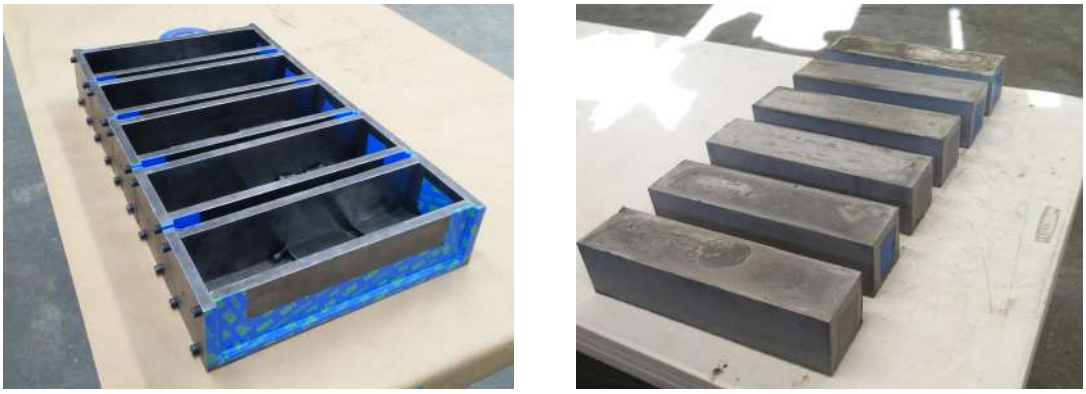

(a) (b)

Figure 3: (a) Steel molds for casting freeze-thaw specimens, (b) Typical freeze-thaw specimens used in ASTM C666 Procedure A.

(a) (b)

Figure 4: (a) Specimens submerged in water inside steel trays, (b) Two environmental chambers with continuous data acquisition system.

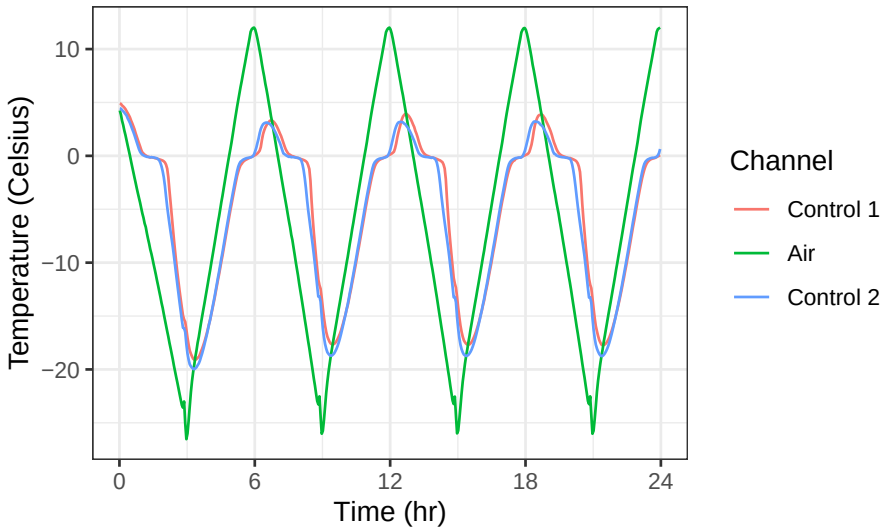

Figure 5: Typical cycles of the two control specimen temperatures and the environmental chamber air temperature.

oscilloscope (Figure 7a). This time domain response is then converted computationally into the frequency domain (Figure 7b) to obtain the frequency corresponding to the resonant peak, i.e., the fundamental frequency.

ASTM C666 defines a dimensionless number to be used as a parameter to make a comparison between different materials, called the durability factor. The durability factor (DF) according to ASTM C666 is defined as:

$$DF = \frac{P \times N}{M} \tag{3}$$

where P is the RDME at N cycles (E/E_0) in %, N is the number of cycles at which P reaches the specified minimum value for discontinuing the test or the specified number of cycles at which the exposure is to be terminated, whichever is smaller, and M is the specified number of cycles at which the exposure is to be terminated.

ASTM C666 Procedure A was performed on four different commercially available high-strength cementitious grouts and one conventional concrete mix. Table 2 provides a summary of the results obtained for the tested grouts. CG1-CG4 stand for cementitious grouts one to four, and PG1 stands for pea-gravel concrete which can be understood to represent the class of conventional flowable concrete ordered from a local ready-mix producer. The water content per bag used for each grout material (CG series) was chosen based on the amount specified by the manufacturer. These water contents are provided in Table 2, presented earlier. All the specimens were cast using a concrete drum mixer with a capacity of 6 ft^3 per batch.

It is clear from Table 2 that most materials performed well and some performed poorly. Figure 8 shows the results of all the materials that were tested. Five identical specimens were cast for each material. For example, for CG1 (Figure 8a), these are labeled as CG101 to CG105. As seen in Figure 8a, since no reduction in E/E_0 was observed, it can be concluded that there was minimal or no damage due to FT cycles. CG2 (Figure 8b) and CG3 (Figure 8c) also showed similar resistance

Figure 6: Experimental setup to determine the fundamental frequency of prismatic specimens.

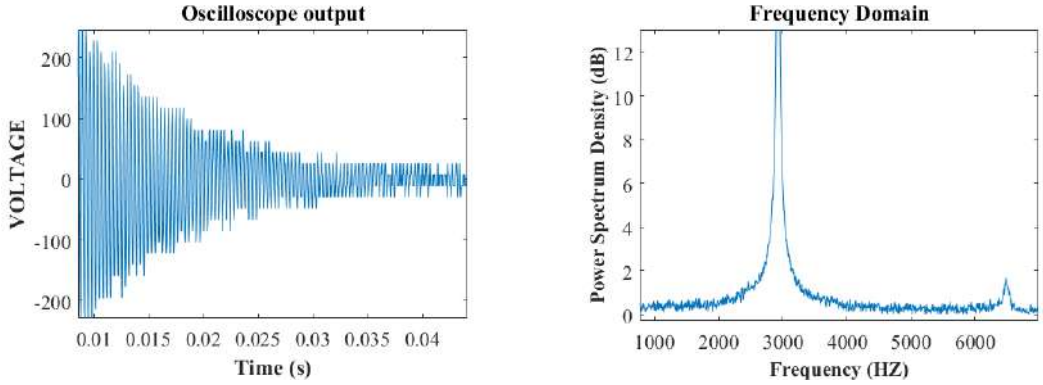

(a) (b)

Figure 7: A typical time domain and frequency domain pair of specimen acceleration responses (a) Time domain (b) Frequency domain.

Table 2: Grout mixtures tested under ASTM C666.

Mixture Code	Water Content per bag (lbs.)	Durability Factor (DF)	Concluding Remarks
CG1	8.5	100%	Good
CG1	9.0	100%	Good
CG2	8.4	100%	Good
CG3	6.6	100%	Good
CG4	9.3	46%	Poor
PG1	w/c = 0.46	<10%	Extremely Poor

to freeze and thaw cracking as that of CG1. Apart from a single specimen showing a slight dip in E/E_0 for CG2, all of the other specimens retained 100% of their initial elastic modulus throughout the 300 cycles. It was concluded that grouts CG1, CG2 and CG3 show good FT resistance and therefore were selected to proceed to the next phase of durability tests, discussed later.

Not all the materials that were tested showed good performance. For example, in CG4 (Figure 8d), there is significant reduction in E/E_0 over time. CG4 was therefore concluded to be more prone to damage due to FT cycles. Figure 8e shows the results for PG1. All specimens of PG1 failed consistently within the first 10 cycles of freeze and thaw. Behavior of PG1, flowable pea-gravel concrete, merits some discussion. The water-cement ratio for this concrete was 0.46. According to the Powers' model [22, 23], a w/c ratio of 0.42 results in all of the water being consumed for the hydration reaction. This implies that a w/c ratio of 0.46 would leave excess water within the microstructure forming capillary pores. Furthermore, the cementitious particles that contributed to the w/c ratio included fly ash, which is pozzolanic in nature and only contributes to the strength of the microstructure in the long term. Hence, the effective w/c ratio during early age would have been some value higher than 0.46 because pozzolanic materials do not take part in the early hydration reaction. This higher w/c ratio results in a larger amount of water filled pores. This may have resulted in early attainment of the critical degree of saturation of the material. The critical degree of saturation of a material is the degree of saturation of the pores inside the material above which freezing of the pore water causes significant cracking. Although a 6% air content was specified within the mixture, which is typically done to increase the freeze-thaw resistance, the mixing may not have achieved a good dispersion of air. A combination of all of the above factors could have caused the observed poor results. Nevertheless, it was decided not to pursue further inquiry into pea-gravel concrete.

After the FT tests, the grouts that showed good performance, viz., CG1, CG2, and CG3 were chosen to be subjected to shrinkage cracking tests. Details of the these tests are discussed next.

2.2. Restrained Shrinkage Cracking of Cementitious Grouts

Portland cement-based materials undergo volume change as a result of the hydration process and consequent loss of moisture. This is called shrinkage. When allowed to shrink freely with no external restraint, no stresses develop within the material. However, concrete or grout materials are commonly restrained against free shrinkage. This restraint causes stress development in the

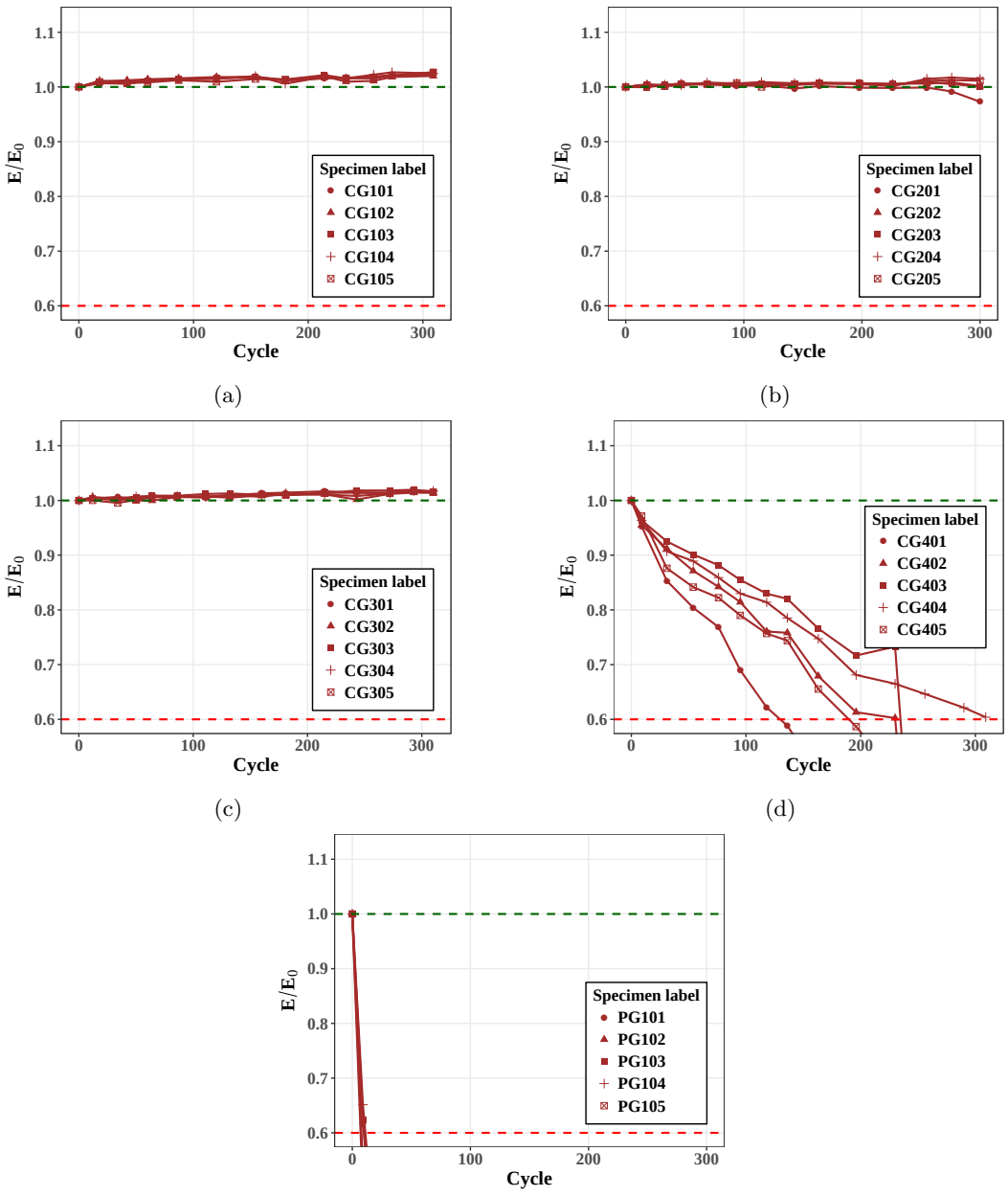

Figure 8: Results from ASTM C666 FT tests on multiple commercial grouts. (a) Grout: CG1, Water per bag: 8.5 lbs, (b) Grout: CG2, Water per bag: 8.4 lbs., (c) Grout: CG3, Water per bag: 6.6 lbs, (d) Grout: CG4, Water per bag: 9.3 lbs., (e) Grout: PG1, w/c ratio: 0.46. .

material. If these stresses exceed the tensile strength of the material, cracking ensues. The potential for cracking depends on the magnitude of these stresses and the tensile strength of the material.

The shrinkage characteristics of the grout are important in the overall performance of the GSS connection because the force transfer occurs through multiple mechanisms dependent on the grout. The size and shape of the annular grouted zone, as well as the restraint provided by the inner steel pipe, may play a role in the long-term performance of the GSS connection.

The standard test to determine the cracking age and the induced tensile stress under restrained shrinkage is ASTM C1581 [24] which is also known as the "restrained ring test" or simply the "ring test". The core aim of the test is to determine the early age cracking tendency of concrete. The concrete material is cast as an annular ring around a circular steel ring. Due to shrinkage of the concrete ring, the imposed strain on the inside steel ring is measured as a function of time. When a crack forms, the tensile stress in the grout is released and a sudden reduction in the compressive strain in the steel ring is observed. When comparing different materials, the earlier a material cracks, the higher is its cracking potential. Similarly, the higher the rate of strain development for a material, the sooner the material will crack. It should be noted that the ring test does not measure a fundamental material property. It rather measures the response of the material to a stimulus under a specific boundary condition. This means that if the boundary conditions (e.g., degree of restraint, drying rate, surface-to-volume ratio) change, the results of the test will also change.

Note the similarity between the specimen geometry of the ring test to the GSS connection. This similarity is coincidental. To investigate shrinkage cracking potential in the GSS connection, the same cross sectional geometry of the GSS connection was used rather than the size specified by ASTM C1581. The degree of restraint of the ASTM C1581 ring is 72.5% while that of the GSS connection was only 64%. It was important to model the degree of restraint in determining the shrinkage cracking potential. The complete test matrix for the restrained ring test is given in Table 3. Three grout materials that performed well in FT tests CG1, CG2, and CG3 were used in the first six ring tests. Each material was subjected to two different drying conditions, viz., circumferential drying and sealed (no drying). The schematic in Figure 9 shows the two different drying conditions. In circumferential drying, the grout ring 3.5" thick, was cast around a 6" tall steel ring of 16" diameter and 0.5" wall thickness, with the top and bottom sealed. To eliminate friction, the grout was separated from the steel ring by an acetate sheet oiled on both sides. The outside surface of the grout ring was exposed to the environment which was controlled at 23°C and 50% relative humidity (RH). Four strain gages were placed on the inside of the steel rings at 90° angles. For specimens under sealed or no drying conditions, the only difference in the setup to that of circumferential drying specimens was that their outer surface was no longer exposed. An outer steel ring covered the grout ring rendering the specimens fully sealed. Again, acetate sheet and oil layers separated the outer ring from the grout. Note that this outer ring did not influence any other characteristics of the test setup. Three specimens of each material (CG1, CG2 and CG3) were tested. The rings were placed inside an environmental chamber for temperature and humidity control. Figure 10 shows a photograph of a sample test setup. The rings in the figure are under circumferential drying conditions.

Figure 11 shows the results for the first six ring tests. The figure is divided into two columns and three rows based on the two drying conditions and three grout materials. The sub-figures have the time (in days) on the x-axis. This is the elapsed time from the moment of casting the grout material. Strain readings averaged over all of the strain gages on one specimen are given on the y-axis. The readings are in micro-strain ($\mu\epsilon$) units. The negative values of strain indicate

Table 3: Test matrix and results for restrained shrinkage ring tests

Test No.	Material	Drying Condition [1]	Shear Studs	Avg. age of cracking (days)	Avg. crack width (mm)
1	CG1	CD	None	3.2	1.70
2	CG2	CD	None	6	1.00
3	CG3	CD	None	5.9	1.08
4	CG1	ND	None	9.5	0.40
5	CG2	ND	None	15.3	0.30
6	CG3	ND	None	N/A	N/A
7	CG1	ND	24-3/4" dia.	7.5	0.10
8	CG1	ND	8-1" dia.	9.9	0.10

[1] CD - Circumferential Drying; ND - Sealed (No Drying)

compression on the inside ring. As time progressed since casting, the strains increased until the point where the grout material cracked. The formation of a crack plane was accompanied by a release of stress which manifested itself in the figures as an instantaneous decrease in steel strain level. It is clear that the circumferential drying condition (Figures 11a, 11c, and 11e) is more severe than no drying (Figures 11b, 11d, and 11f). All the materials cracked earlier under circumferential drying condition compared to no drying. This matched expectations since the stress development inside the material due to restrained shrinkage is proportional to the amount of drying which in turn is proportional to the exposed surface-to-volume ratio of the specimen. Since no surface was exposed for drying in the case of sealed conditions, the stress development was slower.

However, most of the specimens under no drying still cracked, albeit at a later time. All specimens of CG1 and two specimens of CG2 cracked under no drying. None of the specimens of CG3 cracked. In comparison therefore, CG3 performed better than the other two, while CG1 had the highest potential for cracking. The strain at cracking is also an indicator of the cracking potential. CG1 has a higher strain accumulation rate and also cracked at strains much higher than the other two. Since CG1 specimens accumulated high strains even under no drying conditions, it may be concluded that the autogenous shrinkage component is high for CG1. Autogenous shrinkage is the component of shrinkage that occurs without any exposure to the environment [6]. This happens within the grout microstructure as a result of the hydration reaction of cement. Autogenous shrinkage is comparatively lower for CG2 and CG3.

Along with age of cracking and the steel strain at cracking, the crack width of each specimen at 10 days post cracking was also measured. The crack widths were of interest because wider cracks facilitate more ingress of water and chemicals, and can have further deleterious effects. For circumferential drying condition, the crack widths were large for all three materials. CG1 had the highest crack width of 1.70 mm. When tested under no drying condition, the crack widths reduced drastically. This was reassuring since the connection geometry of the GSS connection will result in conditions closer to no drying. Resulting data of average age of cracking and average crack width have been tabulated in Table 3.

The next tests in the series of ring tests were performed to identify the effect of shear studs on the grout cracking potential. Grout material CG1 was chosen to perform these tests as it performed poorest among the three that were tested previously. Even under no drying condition, all specimens

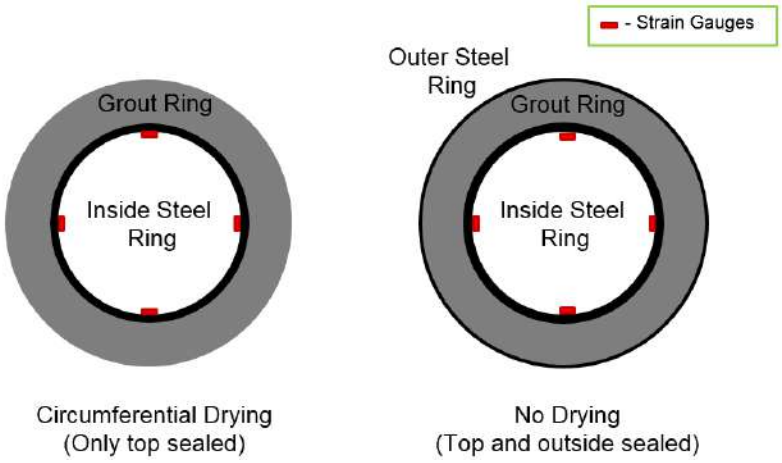

Figure 9: Restrained ring test specimen cross section schematic: Circumferential drying specimen (left) and sealed specimen (right).

of CG1 cracked with an average crack width of 0.40 mm. Upon discussion with personnel from Alaska Department of Transportation and Public Facilities (AKDOT), we learned that a crack width of 0.30 mm is an acceptable upper bound because it can be repaired by epoxy injection. The presence of shear studs within the grout produces two opposing effects with respect to cracking potential of the grout. Shear studs increase the degree of restraint thereby hastening cracking, but simultaneously can create redundant load paths to distribute a single large crack into multiple cracks of reduced width.

Two tests were performed to investigate the effect of shear studs. Each test was performed under no drying condition with two different sizes of shear studs. The first test (Test 7 in Table 3) had 24 shear studs of 3/4" diameter within the grout ring, while the second test (Test 8 in Table 3) had 8 shear studs of 1" diameter. Strain gages were attached on the inside of the steel rings in the regions in between the welded studs. The presence of shear studs likely created a non-uniform distribution of stress (and hence strain) in the steel ring, but it was assumed that an average over all strain gages may still provide meaningful results.

Specimens with both 3/4" diameter and 1" diameter studs showed a release of strain at an average of 7.5 days and 9.9 days, respectively. However, this observation did not correspond to visual cracking on the top surface. Since the release of strain was not towards zero, it was concluded that the shear studs contributed to resistance to cracking. Cracks started to appear on the surface not long after the first instance of stress reduction. Instead of a single crack that was observed in earlier tests without shear studs, multiple cracks formed when shear studs were present. Moreover, these cracks were smaller compared to the wide single cracks observed earlier. This observation led to the conclusion that the shear studs play an important role in reducing crack widths. Further research is necessary to quantify the effect of shear studs on shrinkage cracking. A detailed investigation of this mechanism was beyond the scope of this study.

Among the tests that were conducted under sealed/no drying condition, the results followed an expected trend. The ring specimens with the most number of shear studs (24 studs) cracked the earliest. This result was due to the highest degree of restraint among the three different types of specimen. The rings with the second highest degree of restraint cracked later and those with the

Figure 10: Restrained ring test specimens under circumferential drying conditions in the environmental chamber.

lowest degree of restraint among the three cracked last. A separate observation is that the rings with 24 shear studs cracked at relatively higher stresses in the grout. This can be an indication of the contribution of shear studs to the tensile strength of the grout ring. More tests are needed to confirm this hypothesis.

3. Conclusions

Cementitious grouts from four different manufacturers, all meeting AKDOT requirements, were chosen to assess their strength and durability characteristics. All four grouts developed high early age strength compared to normal concrete, some having much higher strength than the others. After testing the freeze-thaw resistance of chosen grouts, it was found that some grouts were durable and some not. For application in cold climates, grouts have to be chosen with caution.

Early age shrinkage is an inherent characteristic of cementitious materials. All the grouts chosen for restrained ring tests cracked within the first few days after casting. This means that the geometry of the GSS connection provides a high enough restraint to crack high-strength grouts. However, when shear studs were added in the rings, the cracking was delayed and upon cracking, the grout rings formed multiple cracks of smaller widths. This result is, of course desirable. Hence, in addition to the structural contribution, shear studs serve a secondary function of distributing shrinkage cracks and reducing crack widths.

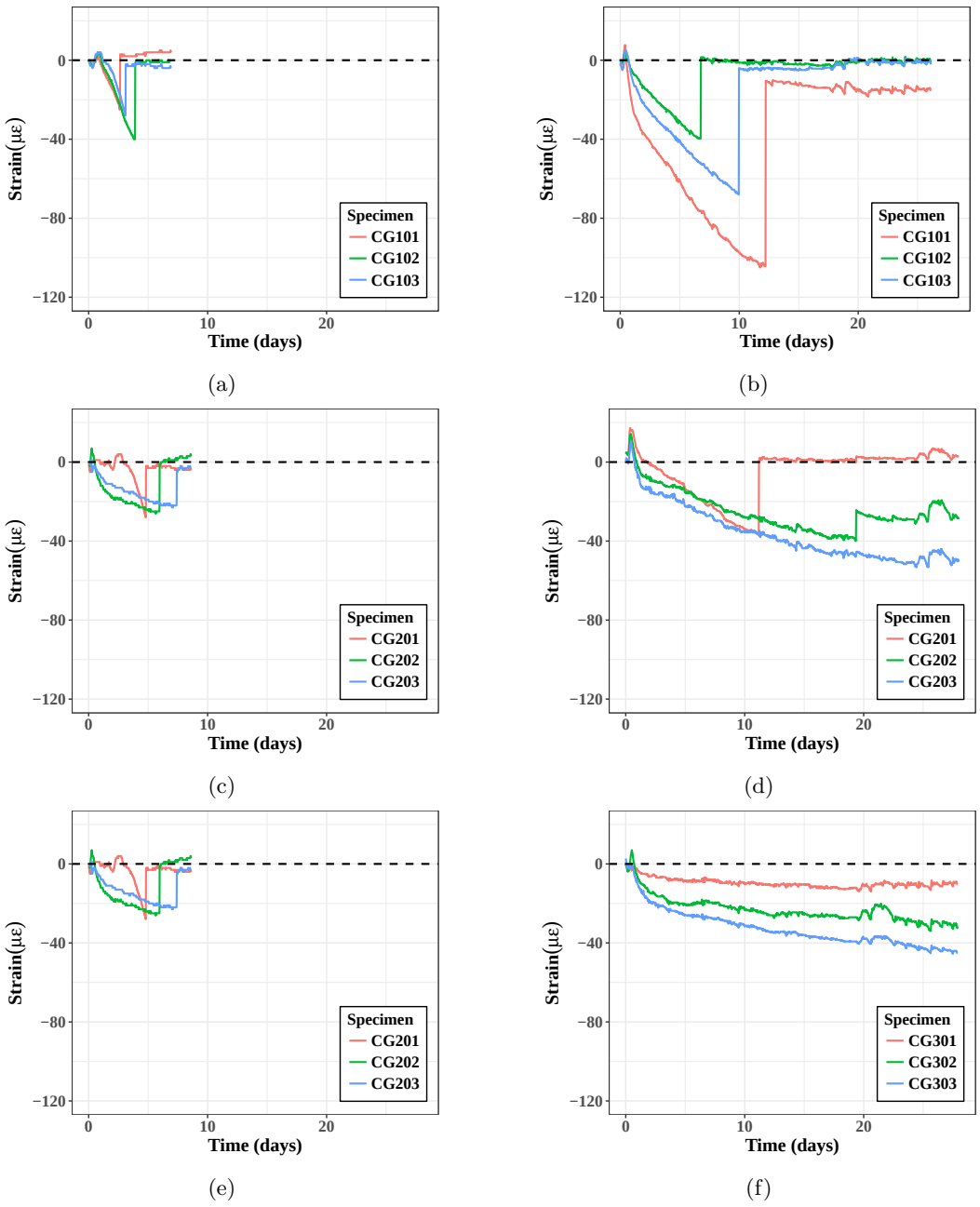

Figure 11: Results from restrained ring tests tests on cementitious grouts under two different drying conditions: CG1 (a) Circumferential drying and (b) Sealed, CG2 (c) Circumferential drying and (d) Sealed, and CG3 (e) Circumferential drying and (f) Sealed conditions.

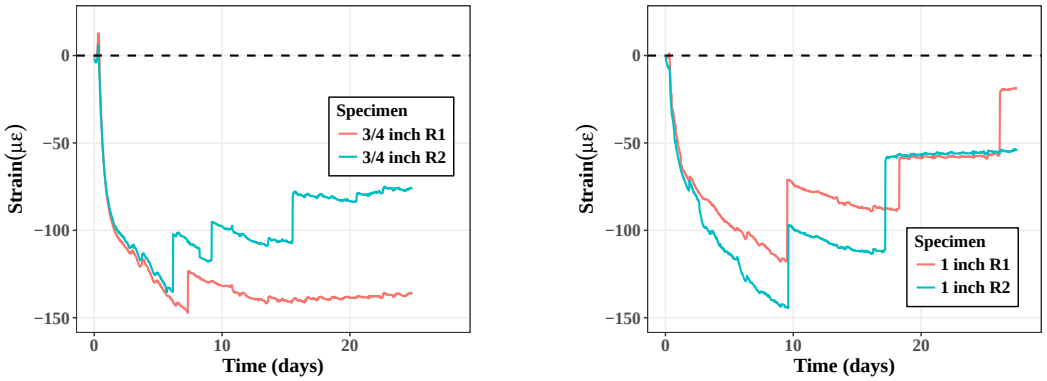

(a) (b)

Figure 12: Results from ring tests performed on specimens with shear studs: (a) 3/4" dia. shear studs (b) 1" dia. shear studs.

References

1. Fulmer S, Kowalsky M, Nau J, Hassan T. Ductility of welded steel pile to steel cap beam connections. In: *Structures Congress 2010*. 2010:216–27.

2. Fulmer SJ, Kowalsky MJ, Nau JM, Hassan T. Ductility of welded steel column to steel cap beam connections. Tech. Rep.; Alaska Department of Transportation and Public Facilities; 2010.

3. Fulmer S, Kowalsky M, Nau J. Grouted shear stud connection for steel bridge substructures. *Journal of Constructional Steel Research* 2015;109:72–86.

4. Litvan G. Freeze-thaw durability of porous building materials. In: *Durability of building materials and components*. ASTM International; 1980:.

5. Litvan GG. The mechanism of frost action in concrete: Theory and practical implications. National Research Council Canada, Institute for Research in Construction; 1988.

6. Mehta PK, Monteiro PJ. Concrete microstructure, properties and materials. 2017.

7. Beaudoin JJ, MacInnis C. The mechanism of frost damage in hardened cement paste. *Cement and Concrete Research* 1974;4(2):139–47.

8. Setzer M. Micro ice lens formation and frost damage. In: *Proceedings of the International RILEM Workshop on Frost damage in concrete, Minneapolis, 28–30 June 1999*. 1999:1–15.

9. Bager D. Qualitative description of the micro-ice body freeze-thaw damage mechanism in concrete. freeze-thaw testing of concrete–input to revision of cen test methods. In: *Workshop proceeding From a Nordic Mini-seminar*. 2010:4–5.

10. Hossain AB, Weiss J. Assessing residual stress development and stress relaxation in restrained concrete ring specimens. *Cement and Concrete Composites* 2004;26(5):531–40.

11. Hossain AB, Weiss J. The role of specimen geometry and boundary conditions on stress development and cracking in the restrained ring test. *Cement and Concrete Research* 2006;36(1):189–99.

12. Li W, Pour-Ghaz M, Castro J, Weiss J. Water absorption and critical degree of saturation relating to freeze-thaw damage in concrete pavement joints. *Journal of Materials in Civil Engineering* 2011;24(3):299–307.

13. Janssen D. Requirements for a test of frost resistance of concrete. In: *International RILEM Workshop on Frost Resistance of Concrete*. RILEM Publications SARL; 2002:277–86.

14. Scherer GW, Valenza J. Mechanisms of frost damage. *Materials science of concrete* 2005;7(60):209–46.

15. Moon JH, Weiss J. Estimating residual stress in the restrained ring test under circumferential drying. *Cement and Concrete Composites* 2006;28(5):486–96.

16. Moon JH, Rajabipour F, Pease B, Weiss J. Quantifying the influence of specimen geometry on the results of the restrained ring test. *Journal of ASTM international* 2006;3(8):1–14.

17. Schlitter JL. New methods to quantify the cracking performance of cementitious systems made with internal curing. Ph.D. thesis; Purdue University; 2010.

18. ASTM C666/C666M-15. Standard Test Method for Resistance of Concrete to Rapid Freezing and Thawing. Standard; ASTM International; West Conshohocken, PA; 2015.

19. ASTM C39/C39M-18. Standard Test Method for Compressive Strength of Cylindrical Concrete Specimens. Standard; ASTM International; West Conshohocken, PA; 2018.

20. ASTM C109/C109M-16a. Standard Test Method for Compressive Strength of Hydraulic Cement Mortars (Using 2-in. or [50-mm] Cube Specimens). Standard; ASTM International; West Conshohocken, PA; 2016.

21. ASTM C215-14. Standard Test Method for Fundamental Transverse, Longitudinal, and Torsional Resonant Frequencies of Concrete Specimens. Standard; ASTM International; West Conshohocken, PA; 2014.

22. Powers TC. Physical properties of cement paste. Tech. Rep.; 1960.

23. Powers TC, Brownyard TL. Studies of the physical properties of hardened portland cement paste. In: *Journal Proceedings*; vol. 43. 1946:101–32.

24. ASTM C1581/C1581M-18. Standard Test Method for Determining Age at Cracking and Induced Tensile Stress Characteristics of Mortar and Concrete under Restrained Shrinkage. Standard; ASTM International; West Conshohocken, PA; 2018.